Phys. Status Solidi B **249,** No. 12, 2315–2322 (2012) / **DOI** 10.1002/pssb.201200134

physica status solidi b
www.pss-b.com
basic solid state physics

Feature Article

Chemical vapor deposition of carbon nanotube forests

J. Robertson*, G. Zhong, S. Esconjauregui, C. Zhang, M. Fouquet, and S. Hofmann

Engineering Department, Cambridge University, Cambridge CB2 1PZ, United Kingdom

Received 2 May 2012, revised 16 August 2012, accepted 11 September 2012
Published online 6 November 2012

Keywords carbon nanotubes, chemical vapor deposition, CNT forest

* Corresponding author: e-mail jr@eng.cam.ac.uk, Phone: +44 1223 748331, Fax: +44 1223 748348

We review the growth mechanisms of vertically aligned carbon nanotube forests, in terms of what controls the growth rate and control of the catalyst lifetime. We also review the production of very high-density forests, in terms of increasing the catalyst particle density.

1 Introduction Carbon nanotubes (CNTs) have many valuable properties. They can be grown by various methods, but chemical vapor deposition (CVD) has become the dominant method, both in the lab and for production. CVD can be used to grow bulk material [1] or to grow on surfaces. Some years ago, it became possible to grow vertically aligned CNT (VACNT) forests [2–5]. The first forests were multiwall nanotubes (MWNTs), showing that Fe was an excellent catalyst, especially on Al_2O_3 as a support layer [6].

One of the drawbacks of bulk growth was the impurity of the product in terms of both amorphous carbon, graphitic carbon, and encapsulated catalyst, which could not easily be removed. Hata et al. [7] observed that hydrogen diluted ethylene together with a mild etchant, water, and the Fe/Al_2O_3 catalyst/support combination led to extremely efficient growth, with roughly 1 nm of catalyst leading to 1–10 mm high CNT forests, a yield of roughly 10^6. This method followed similar work on single-walled carbon nanotubes (SWNTs) forests [8–12].

It is now of interest to understand the limits to forest growth, their growth mechanism in terms of a rate limiting step, and finally to study extensions of forest growth to cases of very high density growth or lower density forests with novel rubber-like properties.

2 Growth mechanism The CNTs grow by a three-stage process; first the catalyst is deposited, the catalyst then restructures into nanoparticles, then the CNT nucleates and grows from the catalyst particle (Fig. 1). In CVD, one CNT grows from each catalyst particle.

The combination of an Fe catalyst and Al_2O_3 support layer was discovered empirically from growing MWNTs forests. Previously, SiO_2 was used as a support layer and could grow forests under some conditions [1]. The vertically aligned growth of forests is attributed to many CNTs growing in close proximity to each other, causing them all to grow vertically.

SWNTs grow faster than MWNTs because the growth rate depends on carbon diffusion and this varies inversely with CNT diameter [13–15]. Thus, as the fastest growing species, SWNTs provide the best opportunity to make the purest CNTs by growing fastest.

The most effective growth requires a combination of fast growth and keeping the catalyst active for the longest time. A number of groups were able to develop SWNT forest growth. Hata et al. [7, 16] emphasized the role of water as a mild etchant. Various groups tried to maximize the growth height of forests [17–24]. They analyzed the growth kinetics, growth rates, and growth termination mechanism. Yamada et al. [16] attributed growth termination to the encapsulation of the catalyst nanoparticle by amorphous carbon. Water was observed by electron energy loss spectroscopy to etch away any a-C covering the catalyst particles, and so prolong the lifetime of the catalyst [16] (Fig. 2). The growth rate can follow an exponential decay [17] but sometimes, the growth termination is more abrupt. Amama et al. [21, 22] noted that the catalyst lost activity because of its sintering, Ostwald ripening and its diffusion into the support layer (Fig. 3). Water had the effect of reducing the surface diffusion rate of the catalyst, and so could delay its poisoning.

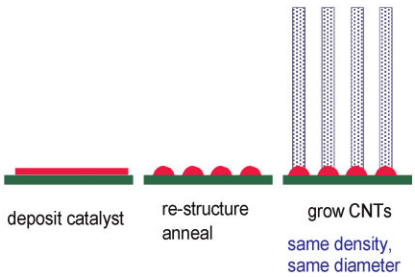

Figure 1 (online color at: www.pss-b.com) Schematic growth process; catalyst deposition, pre-treatment, and growth steps [63].

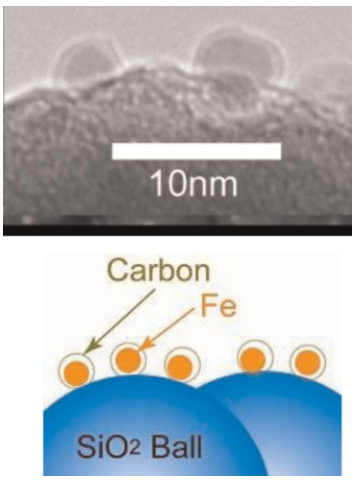

Figure 2 (online color at: www.pss-b.com) High-resolution TEM image and schematic of a-C encapsulating the catalyst nanoparticle, which is then etched off by water [16].

It should be noted that both termination mechanisms are possible, and are likely to operate in different temperature ranges. There is experimental evidence for both processes, but the a-C route may be more general.

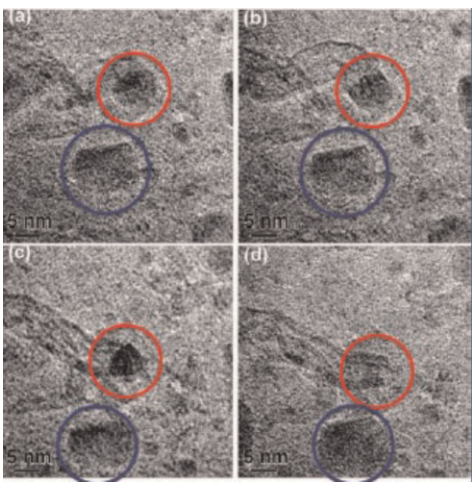

Figure 3 (online color at: www.pss-b.com) TEM cross sectional image showing Fe nanoparticles embedded in Al_2O_3 support layer [22].

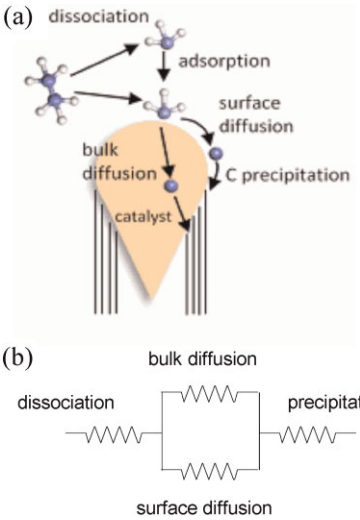

Figure 4 (online color at: www.pss-b.com) (a) Microscopic steps of growth process; gas phase, chemisorption, carbon diffusion, and precipitation of carbon to form the CNT. (b) Showing these steps as sequential process to define the rate-limiting step as the slowest process with the largest activation barrier.

The next question concerns the growth rate itself. Various process effects can affect growth rate. Shower heads and other flow spreading devices are useful to minimize the mass transport limitations [25]. Hot wall systems at higher temperatures cause a reaction of the process gas to form active precursors such as acetylene [26]. The etchant can be any oxygen-containing molecule, if the process gas is used in a hot wall system [27]. On the other hand, hot wire systems and rapid heating in cold wall systems are valuable to rapidly activate the catalyst, to inhibit sintering [28].

Growth consists of a series of sequential processes; transport and possible reaction in the gas phase, dissociative chemisorption on the catalyst surface, diffusion through or over the surface of the catalyst, and finally precipitation out of the nanotube (Fig. 4). The slowest process is the rate-determining step [29]. Work on carbon nanofibers identified that carbon diffusion across the catalyst nano-particle was the rate-limiting step in that case, based on the similarity of the activation energy of growth to that of carbon diffusion [14, 30]. On the other hand, it is well known that CNT growth rates depend at least by a factor of 1000 on the state of the catalyst and on the gas environment. This means that surface processes must be relevant. Eres et al. [31] noted that C_2H_2 was the primary growth species for CNTs, and this has been confirmed by other groups. Wirth et al. [29] determined the dependence of CNT growth rate on the C_2H_2 partial pressure and the growth temperature in a cold wall system. They found that the growth rate varied as the C_2H_2 partial pressure to the half power over six orders of magnitude, Fig. 5a. Also, the activation energy is of order 0.9–1.0 eV, Fig. 5b. This activation energy has been found by others. However, sometimes much higher activation energies are found, when

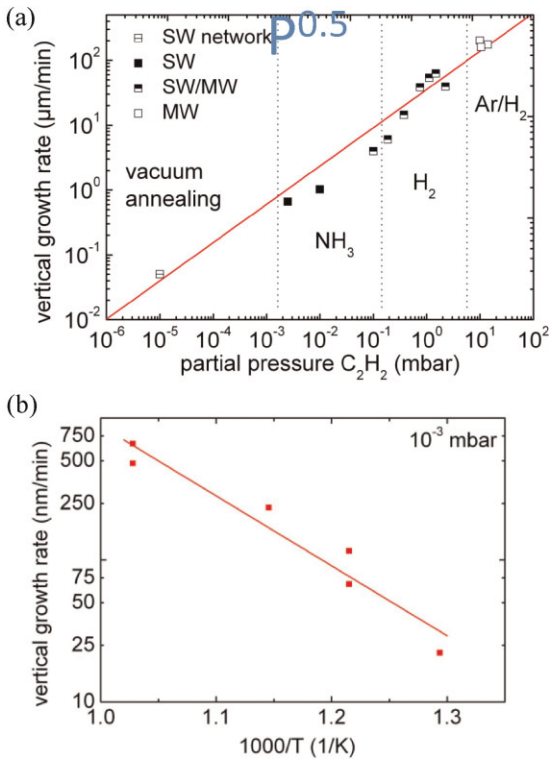

Figure 5 (online color at: www.pss-b.com) (a) CVD growth rate versus C_2H_2 partial pressure in a cold wall CVD system. (b) Temperature dependence, giving activation energy of 0.95 eV [29].

other precursors are used or in hot wall systems. These arise because the activation energy over a small temperature range is dominated by a gas phase reaction that creates the primary growth species C_2H_2 from the feed stock gas. We think that this leads to the high activation energies seen by others in such systems [32–34]. Cold wall systems give only the mechanism of the catalyst itself.

The pressure and temperature dependence can be interpreted as a "pre-equilibrium" of C_2H_2 on the catalyst surface, Fig. 6, before the rate-determining step of carbon

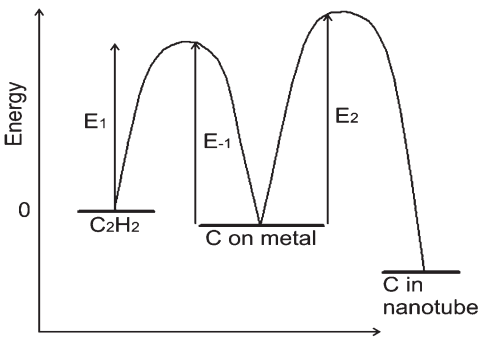

Figure 6 Schematic of energy barriers versus reaction coordinate for CNT growth. Carbon diffusion in/on the catalyst is large barrier (E_2), preceded by a pre-equilibrium step of molecular dissociation on the catalyst surface [29].

diffusion across or over the surface of the catalyst nanoparticle [29]. This model is standard chemical kinetics.

Recently, Yacobson and coworkers [35] developed a model of the growth of SWNTs from the catalyst surface, in terms of its chiral angle. They noted that an energy barrier to precipitation of the CNT rose for chiral angles towards the zigzag. This was noted to correlate with chiral angle abundances found by numerous growth methods – the CVD, laser, or arc methods.

There are two basic mechanisms that can lead to chiral selectivity. Either the chirality is fixed at growth by the nucleation of a cap of certain chirality [36, 37], and then essentially fixed for subsequent growth. Or, the nucleation is less important, and abundances depend on relative growth rates only, as competition during the growth phase.

Rao et al. [38] measured growth rates against chirality by arranging growth of SWNTs dilutely spread over arrays of Si pillars. The chirality was determined by the radial breathing modes (RBMs), then the growth rates were determined from the G band intensity. This experiment gave clear data that the growth rate increased from zigzag to armchair. It thus supports the idea that growth rate is determined by the precipitation rate, as only this can vary with chirality.

We are left with a problem, in chemical kinetics terms, there cannot be *three* rate-limiting steps, only *one*. It is possible to have diffusion as rate-limiting, combined with a pre-equilibrium to include surface processes. But one cannot combine with a *subsequent* step of precipitation in a sequential process. This needs to be resolved by for example measuring the temperature or pressure dependence of growth rates in the Raman experiment.

We can consider the CVD CNTs in terms of a generic heterogeneous reaction of hydrocarbons on a transition metal catalyst surface. There are well known scaling rules linking activation energy to the binding energy of intermediate species. This leads to a "volcano plot" of catalyst efficiency versus transition metal 3d energy [39], as in Fig. 7.

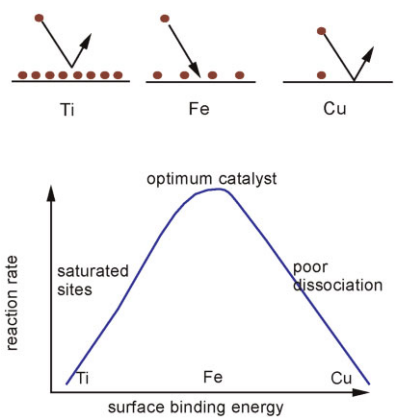

Figure 7 (online color at: www.pss-b.com) Volcano plot of CVD reaction rate versus transition metal d-band energy. Ti is poor catalyst as its surface sites are saturated, Fe is a good catalyst as having open sites. Cu is poor catalyst in being too slow to dissociate hydrocarbons.

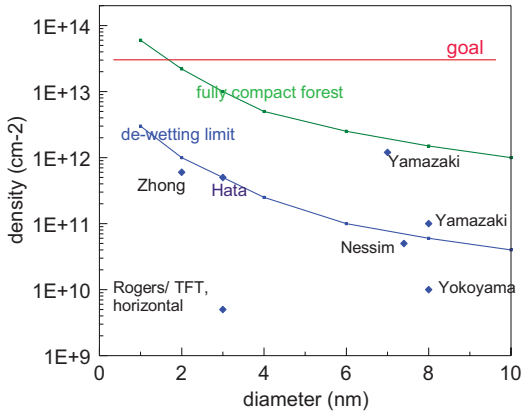

Figure 8 (online color at: www.pss-b.com) Variation of area density with nanotube diameter, for some high density, vertically aligned nanotube forests grown by various groups [51].

3 Catalyst preparation and forest density VACNT forests are impressive in terms of their height. However, on further thought, their density is not so large. Liquid-induced compaction was used by Futaba et al. [40] to estimate their space filling and found that their forests were only about 5% of the maximum theoretical density. Zhong et al. [41] used weight gain to estimate a similar density in their VACNT forests. Other groups get similar or lower values [42, 43]. The area densities are summarized in Fig. 8 where it is seen that standard forests have an area density of $5–7 \times 10^{11}$ cm^{-2} and a mass density of typically 0.05 g cm^{-3}. This density is important for some applications. For example, the thermal conductivity of a single CNT is higher than that of diamond, along a single axis. But the thermal conductivity of a CNT mat, only 5% dense, will be 15 times less than that of diamond [44, 45]. Of course, it is flexible and has other attributes, but as a thermal interface material, it is not as good as first impressions suggest. Similarly, for using CNTs as electrical interconnects in VLSI integrated circuits [46–48]. A low conductivity will require near complete space filling by the CNTs. How can we grow such dense CNT forests?

We return to the observation that each catalyst nanoparticle generates one CNT in CVD (Fig. 1). Thus, to increase the area density of CNTs, we must increase the density of catalyst nanoparticles. One way to do this is by cluster beam deposition [49]. But this is a costly process, and not so suitable for large area substrates without some rastering.

The present process to make the catalyst nanoparticles relies on a lucky break. Catalysts are metals with large surface energy, support layers are typically ionic oxides with low surface energies [48, 50]. Thus, a metal over-laying an oxide layer can lower its total surface energy by breaking up into a series of balls, so exposing the underlying low surface energy support layer. The diameter of the balls is proportional to the initial thickness of the metal layer [48], typically

$$D \sim 6h. \tag{1}$$

Thus, the density of the metal balls will vary inversely with their diameter squared,

$$N \sim \frac{1}{D^2}, \tag{2}$$

and thus with the initial thickness squared,

$$N \sim \frac{1}{h^2}. \tag{3}$$

The simplest way to increase N is to decrease the nanotube diameter by decreasing h [48].

We have studied three ways of increasing N; further details can be found elsewhere [51–53, 48]. The first is to decrease h. Growth of typical forests already uses catalyst films that are very thin, $h \sim 1$ nm. This means that much of the catalyst can diffuse into the support layer during heating and be lost for growth. Al_2O_3 was chosen as a support layer because it has a low surface diffusion [54], but it can be porous, so inward diffusion is possible. To increase N, we must decrease h further. One way to achieve this is to use a plasma to densify the Al_2O_3 support layer [52]. The effect of this is seen in Fig. 9 in SIMS data on the inward diffusion of

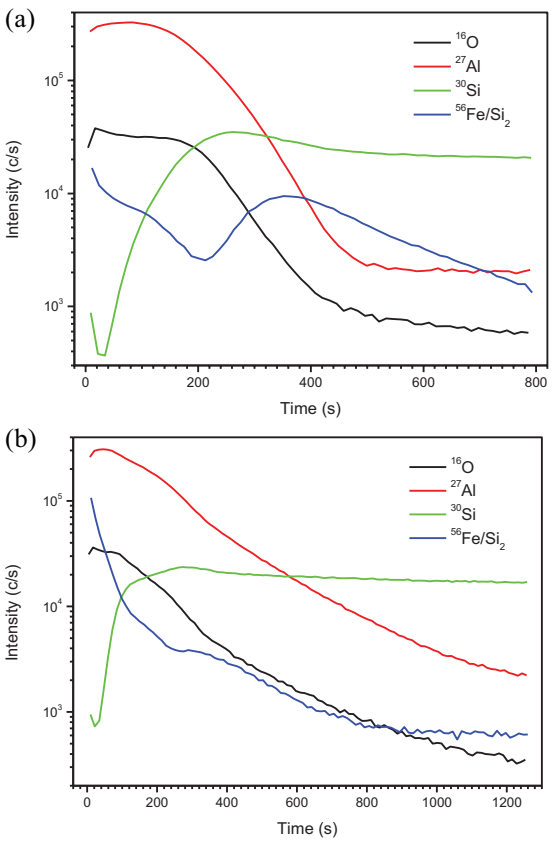

Figure 9 (online color at: www.pss-b.com) SIMS depth profile into a layer of 0.4 nm Fe on 5 nm Al_2O_3 on Si wafer, for case of (a) normal Al_2O_3, and (b) plasma oxidation densified Al_2O_3 [52].

Fe. Figure 8a shows that there is a peak in the Fe diffusion profile where it hits the Si substrate, evidence for inward Fe diffusion, but this is missing when densified Al_2O_3 is used, in Fig. 9b. This allows the use of Fe layers of thickness down to 0.3 nm. In addition, to ensure maximum nucleation from the catalyst nanoparticles, the partial pressure of the growth gas acetylene has been increased.

Figure 10 shows TEM images of the resulting nanotubes. They are SWNTs, and their average diameter is found to be 1.1 nm. This is much less than the typical 2–3 nm. Figure 10a–d shows SEM images of the sides of the forest. The CNTs are well aligned. The area density is largely uniform over the forest, but it is lower at the forest base, just above the catalyst. This is because growth has terminated due to poisoning of catalyst particles. It can be prevented by turning off the growth, not allowing it to terminate. Figure 10f shows the diameter distribution evaluated from Fig. 10e, with an average diameter of 1.1 nm. Figure 11 shows the RBM spectra in resonant Raman, which confirms the diameter distribution from TEM. Figure 11b shows a Raman spectrum with a high G/D ratio.

The area density was measured by weight gain. The sample's weight gain during growth is measured by microbalance, together with the area and height of the forest. Then the CNT diameter is derived from TEM images, for SWNTs and for each wall for MWNTs. This is used to calculate the weight per unit length of the nanotube. The area density is then calculated from the ratio of weight gain to weight per unit length. This gives an area density of order $1.4 \times 10^{13}\,\mathrm{cm}^{-2}$ for the 1.1 nm diameter tubes, Fig. 12. Thus, the density has been increased by a factor of 30.

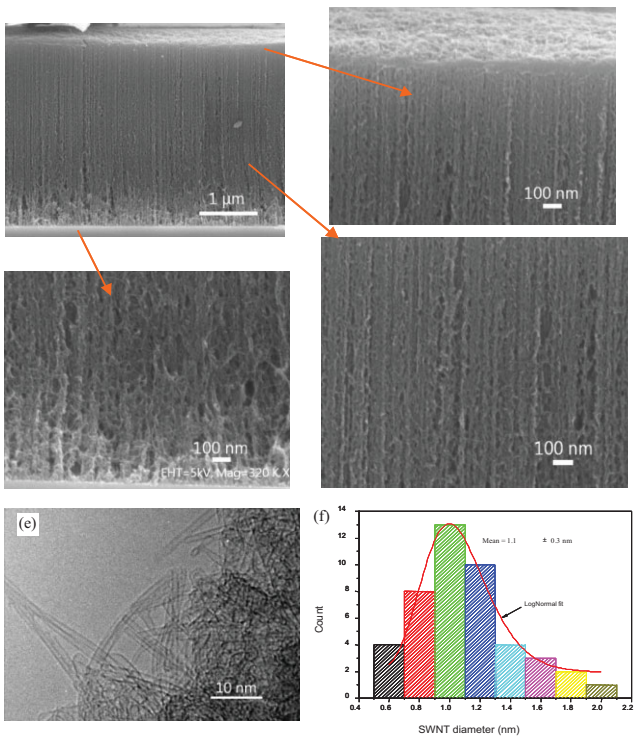

Figure 10 (online color at: www.pss-b.com) (a–d) SEM images of the sides of a high-density forest grown on densified Al_2O_3 for 0.4 nm Fe catalyst, at 8% C_2H_2 in H_2, 20 mbar gas pressure, at 680 °C. (e) High-resolution TEM image of the nanotubes showing them to be mainly single walled. (f) Histogram of diameter distribution [52].

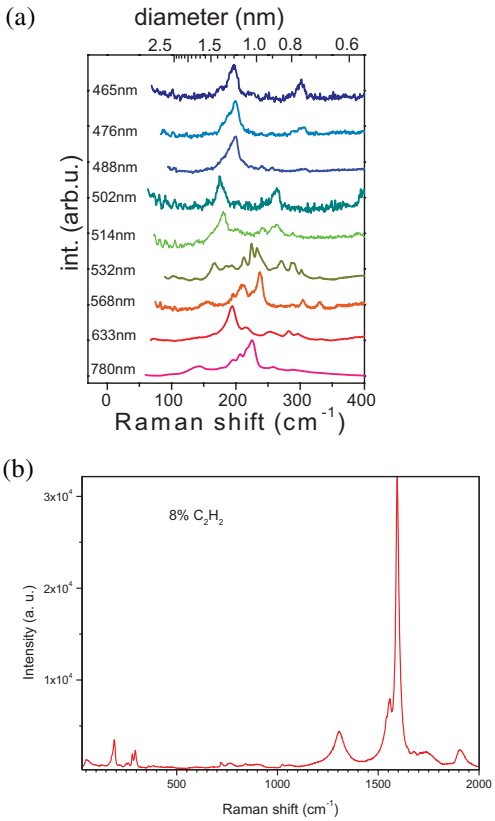

Figure 11 (online color at: www.pss-b.com) (a) Resonant Raman spectra of radial breathing modes (RBMs) of the forest shown in Fig. 10, and the diameter distribution from mode assignments, showing that the nanotube diameters are mostly below 1.5 nm [52]. (b) Raman spectra showing the G and D bands.

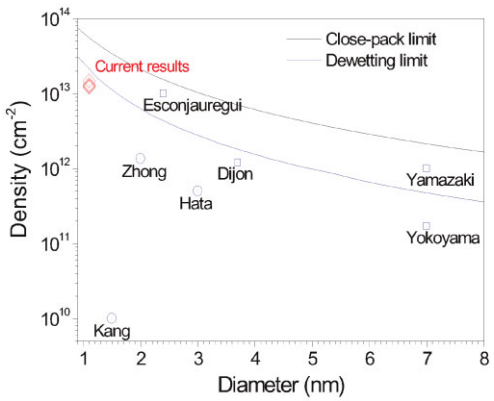

Figure 12 (online color at: www.pss-b.com) Measured densities of forests grown on the densified Al_2O_3 support layer, and by the cyclic catalyst deposition process.

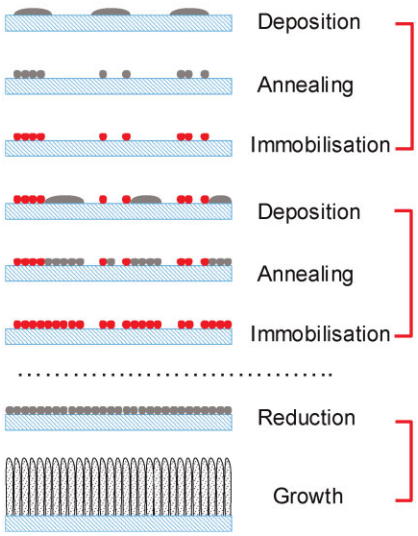

Figure 13 (online color at: www.pss-b.com) Schematic of the cyclic catalyst deposition process.

A second way to increase the area density is to use multi-cycle catalyst deposition [48, 51], as shown schematically in Fig. 13. Equation (1) says that thicker catalysts give thicker CNTs and lower densities. If we deposit two layers of catalyst, annealing would normally sinter these together into a single layer with larger diameter and lower density. However, it is sometimes possible to restructure the first layer by annealing, then, after cooling back to room temperature, depositing a second catalyst layer and annealing this to avoid it sintering into the previous layer. This requires the first layer to be immobilized, so that it does not join with the next layer. If this can be done, then the density can be increased linearly with a number of cycles.

Figure 14 shows a TEM image of the CNTs from this process, showing a diameter of 2.4 nm, and mainly double-walled CNTs. The weight gain method has found an area

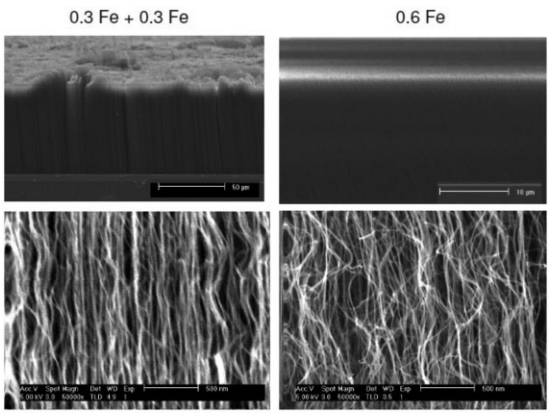

Figure 14 Transverse SEM images of CNTs grown by a two-layer catalyst (left) and single-layer catalyst (right) [51].

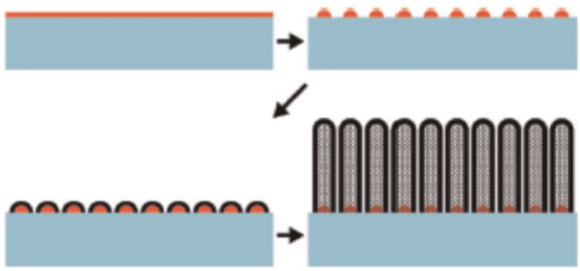

Figure 15 (online color at: www.pss-b.com) Schematic of the three-step catalyst pre-treatment method used by Yamazaki to increase nucleation density.

density of about $1.3 \times 10^{13}\,\mathrm{cm}^{-2}$ for this method. This is also a very high number, and an increase of order 25 over previous densities.

A third method for increasing CNT density developed by Yamazaki et al. [43] involves a three-step process, shown schematically in Fig. 15. The first step uses an Ar plasma to restructure the catalyst into nanoparticles. The second step uses a short hydrocarbon plasma to deposit a thin layer of carbon, which immobilizes the catalyst nanoparticles. Then the growth proceeds as normally. The original work [43] claimed a density of $10^{12}\,\mathrm{cm}^{-2}$, as determined by counting, for MWNTs of diameter of ~7 nm. We have repeated their process, and achieved a smaller diameter of 4 nm and a density of over $10^{12}\,\mathrm{cm}^{-2}$ as determined by weight gain [53]. The results are summarized in Fig. 12. Thus, the three methods each achieve the goal of larger area densities.

It is interesting that the mass density can be related to the area density for the typical and fully compact forest, in terms of the average CNT diameter, as shown in Fig. 16. A fully compact forest is defined as one in which the CNTs are arranged on a hexagonal grid, and separated by 0.34 nm, the graphite *c*-axis spacing.

The present experiments have been carried out in Si wafer substrates. They are being generalized to rougher substrates. It should be noted that the processes invoked depend largely of surface energy effects, layer compaction by ion beams, etc, and should carry over to less smooth surfaces. If necessary, Al_2O_3 can be deposited by atomic layer deposition, which is conformal on any substrate.

It should be noted that the height of the ultra-dense forests is less than the standard forests [52, 53]. This might be due to restricted gas access to the catalyst at the root or it could be due to a short growth life; further experiments are needed to confirm this.

Plasma pre-treatment of the catalyst can be used to enforce the root growth mode, which seems to be a requirement for obtaining the high-density vertically aligned forests [55–57]. Extensive *in situ* XPS and XRD have been used to monitor the chemical state of the catalyst and support layers during growth process [54]. This checks whether the support metals are present as metals or oxides, and whether it is amorphous or crystalline. Another important factor for

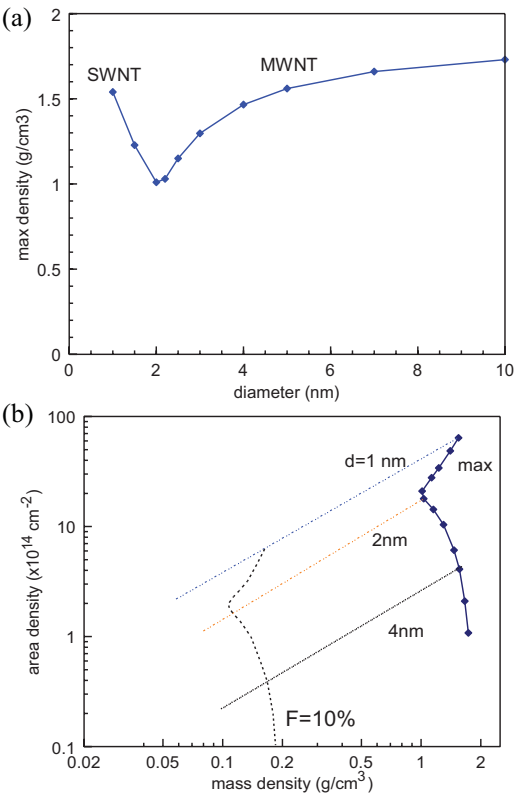

Figure 16 (online color at: www.pss-b.com) (a) Typical variation of mass density of a fully compact CNT forest versus CNT diameter, showing the cross-over from SWNTs to MWNTs. (b) Mass density versus area density for a fully compact forest versus CNT diameter, and also for a forest of 10% fill factor. A fully compact forest is defined as one in which the CNTs are arranged on a hexagonal grid, and separated by 0.34 nm, the graphite *c*-axis spacing.

many applications is the ability to grow on metal or conducting substrates. This can be important for low cost [58], or because the CNTs are being used as conductors [46]. The problems arise because it is less easy to make the catalyst form nanoparticles as in Fig. 1 on metal support layers and sometimes various tricks must be used [59–63].

4 Sparse forests Xu et al. [64] have developed sparse forests, the opposite extreme. In this case, an Ar plasma is used to thin out the catalyst nanoparticles, and thus lower the nanotube's area density. If taken too far, this results in nanotube spaghetti. Before this stage, the nanotubes make a sparsely packed forest, in which the nanotubes are more wavy, but still grow upwards. If the CNTs link together when they touch, they form a rubber-like network. The mechanical and visco-elastic properties have been studied. In contrast to normal rubber, the novelty of "CNT rubber" is that it maintains its visco-elastic properties over a very wide temperature range.

Acknowledgements We thank the EC Technotubes project for funding, K. Hata, D. Futaba, and R. Schlögl for discussions.

References

[1] Y. Li, I. A. Kinloch, and A. H. Windle, Science **304**, 276 (2004).
[2] S. S. Fan, M. G. Chapline, N. R. Franklin, T. W. Tombler, A. M. Cassell, and H. Dai, Science **283**, 512 (1999).
[3] G. Eres, A. A. Puretzky, D. B. Geohegan, and H. Cui, Appl. Phys. Lett. **84**, 1759 (2004).
[4] X. Li, A. Cao, Y. J. Jung, R. Vajtai, and P. M. Ajayan, Nano Lett. **5**, (1997). (2005.
[5] M. Pinault, V. Pichot, H. Khodja, P. Launois, C. Reynaud, C. Reynaud, and M. M. L'Hermitage, Nano Lett. **5**, 2394 (2005).
[6] L. Delzeit, C. V. Nguyen, B. Chen, A. Cassell, J. Han, and M. Meyyappan, J. Phys. Chem. B **106**, 5629 (2002).
[7] K. Hata, D. N. Futuba, K. Mizuno, T. Namai, M. Yumura, and S. Iijima, Science **306**, 1362 (2004).
[8] Y. Miyauchi, S. Chiashi, Y. Murakami, Y. Hayashida, and S. Maruyama, Chem. Phys. Lett. **387**, 198 (2004).
[9] G. Zhong, T. Iwasaki, K. Honda, Y. Ohdomari, and H. Kawarada, Jpn. J. Appl. Phys. **44**, 1558 (2004).
[10] L. Zhang, Y. Tan, and D. E. Resasco, Chem. Phys. Lett. **422**, 198 (2006).
[11] M. Cantoro, S. Hofmann, S. Pisana, V. Scardaci, A. Parvez, C. Ducati, A. C. Ferrari, A. M. Blackburn, K. Y. Wang, and J. Robertson, Nano Lett. **6**, 1107 (2006).
[12] S. Noda, K. Hasegawa, H. Sugime, K. Kazunori, Z. Zhang, S. Maruyama, and Y. Yamaguchi, Jpn. J. Appl. Phys. **46**, L399 (2007).
[13] S. Hofmann, M. Cantoro, B. Kleinsorge, C. Casiraghi, A. Parvez, J. Robertson, and C. Ducati, J. Appl. Phys. **98**, 034308 (2005).
[14] J. Rostrup-Nielsen and D. R. Trimm, J. Catal. **48**, 155 (1977).
[15] C. T. Wirth, S. Hofmann, and J. Robertson, Diam. Relat. Mater. **18**, 940 (2009).
[16] T. Yamada, A. Maigne, M. Yudasaka, K. Mizuno, D. N. Futaba, M. Yumura, S. Iijima, and K. Hata, Nano Lett. **8**, 4288 (2008).
[17] D. N. Futaba, K. Hata, T. Yamada, K. Mizuno, M. Yumura, and S. Iijima, Phys. Rev. Lett. **95**, 056104 (2005).
[18] G. F. Zhong, T. Iwasaki, J. Robertson, and H. Kawarada, J. Phys. Chem. B **111**, 1907 (2007).
[19] R. Xiang, Z. Yang, Q. Zhang, G. Luo, W. Qian, F. Wei, M. Kadowaki, E. Einarsson, and S. Maruyama, J. Phys. Chem. C **112**, 4892 (2008).
[20] E. R. Meshot and A. J. Hart, Appl. Phys. Lett. **92**, 113107 (2008).
[21] P. B. Amama, C. L. Pint, L. McJilton, S. M. Kim, E. A. Stach, P. T. Murray, R. H. Hauge, and B. Maruyama, Nano Lett. **9**, 44 (2009).
[22] S. M. Kim, C. L. Pint, P. B. Amama, D. N. Zakharov, R. H. Hauge, B. Maruyama, and E. A. Stach, J. Phys. Chem. Lett. **1**, 918 (2010).
[23] P. Vinten, P. Marshall, J. Lefebvre, and P. Finnie, Nanotechnology **21**, 035603 (2010).
[24] K. Hasegawa and S. Noda, Jpn. J. Appl. Phys. **49**, 085104 (2010).
[25] S. Yasuda, D. N. Futaba, and K. Hata, ACS Nano **3**, 4164 (2009).
[26] G. Zhong, S. Hofmann, F. Yan, H. Telg, J. H. Warner, D. Eder, C. Thomsen, W. I. Milne, and J. Robertson, J. Phys. Chem. C **113**, 17321 (2009).

[27] D. Futaba, J. Gato, S. Yasuda, T. Yamada, M. Yumura, and K. Hata, Adv. Mater. **21**, 4811 (2009).
[28] C. L. Pint, S. T. Pheasant, A. Parra-Vasquez, C. Horton, Y. Q. Xu, and R. H. Hauge, J. Phys. Chem. C **113**, 4125 (2009).
[29] C. T. Wirth, C. Zhang, G. Zhong, S. Hofmann, and J. Robertson, ACS Nano **3**, 3560 (2009).
[30] R. T. K. Baker, J. Catal. **26**, 51 (1972).
[31] G. Eres, A. A. Kinkhabwala, H. Cui, D. B. Geohegan, A. A. Puretzky, and D. H. Lowdnes, J. Phys. Chem. B **109**, 16684 (2005).
[32] A. A. Puretzky, D. B. Geohegan, S. Jesse, I. N. Ivanov, and G. Eres, Appl. Phys. A **81**, 223 (2005).
[33] R. Xiang, E. Einarsson, J. Okawa, Y. Miyauchi, and S. Maruyama, J. Phys. Chem. C **113**, 7511 (2009).
[34] M. Picher, E. Anglaret, R. Arenal, and V. Jourdain, Nano Lett. **9**, 542 (2009).
[35] F. Ding, A. Haratyunyan, and B. Yacobson, Proc. Natl. Acad. Sci. USA **106**, 2506 (2009).
[36] S. Reich, L. Li, and J. Robertson, Chem. Phys. Lett. **421**, 116 (2006).
[37] H. Zhu, K. Suenaga, A. Hashimoto, K. Urita, K. Hata, and S. Ijima, Small **1**, 1180 (2005).
[38] R. Rao, D. Liptak, T. Cherukuri, B. I. Yacobson, and B. Maruyama, Nature Mater. **11**, 213 (2012).
[39] J. Robertson, J. Mater. Chem. **22**, 19858 (2012).
[40] D. N. Futaba, K. Hata, T. Yamada, T. Hiraoka, Y. Hayamizu, Y. Kakudate, O. Tanaike, H. Hatori, M. Yumura, and S. Iiijima, Nature Mater. **5**, 987 (2006).
[41] G. Zhong, T. Iwasaki, and H. Kawarada, Carbon **44**, 2009 (2006).
[42] D. Yokoyama, T. Iwasaki, K. Ishimaru, S. Sato, T. Hyakushima, M. Nihei, Y. Awano, and H. Kawarada, Jpn. J. Appl. Phys. **47**, 1985 (2008).
[43] Y. Yamazaki, N. Saluma, M. Katagiri, M. Suzuki, T. Sakai, S. Sato, M. Nihei, and Y. Awano, Appl. Phys. Express **3**, 55002 (2010).
[44] X. J. Hu, A. A. Padilla, J. Xu, T. S. Fischer, and K. E. Goodson, J. Heat Transfer **128**, 1109 (2006).
[45] M. Akoshima, K. Hata, D. N. Futaba, K. Mizuno, and M. Baba, Jpn. J. Appl. Phys. **48**, 05EC07 (02009).
[46] Y. Awano, S. Sato, M. Nihei, T. Sakai, Y. Ohno, and T. Mizutani, Proc. IEEE **98**, 2015 (2010).
[47] J. Dijon, H. Okuno, M. Fayolle, J. Pontcharra, A. M. Ionescu, B. Capraro, C. S. Esconjauregui, and J. Robertson, Tech. Digest IEDM (2010), p32.6.
[48] J. Robertson, G. Zhong, C. S. Esconjauregui, B. C. Bayer, C. Zhang, M. Fouquet, and S. Hofmann, Jpn. J. Appl. Phys. **51**, 01AH01 (2012).
[49] S. Sato, A. Kawabata, M. Nihei, and Y. Awano, Chem. Phys. Lett. **382**, 361 (2003).
[50] S. Noda, H. Sugime, and K. Hasegawa, Jpn. J. Appl. Phys. **49**, 02BA02 (2010).
[51] S. Esconjauregui, M. Fouquet, B. C. Bayer, C. Ducati, R. Smajda, S. Hofmann, and J. Robertson, ACS Nano **4**, 7431 (2010).
S. Esconjauregui et al., submitted to J. Phys. Chem. C (2012).
[52] G. Zhong, J. H. Warner, M. Fouquet, A. W. Robertson, B. Chen, and J. Robertson, ACS Nano **6**, 2893 (2012).
[53] C. Zhang, unpublished work.
[54] C. Mattevi, C. T. Wirth, S. Hofmann, R. Blume, M. Canotro, C. Ducati, C. Cepek, A. Knop, S. Milne, C. Castellarin-Cudia, S. Dolafi, A. Goldoni, R. Schlogl, and J. Robertson, J. Phys. Chem. C **112**, 12207 (2008).
[55] J. Dijon, A. Fournier, P. D. Szkutnik, H. Okuno, C. Jayet, and M. Fayolle, Diam. Relat. Mater. **19**, 382 (2010).
[56] S. Esconjauregui, B. C. Bayer, C. T. Wirth, S. Hofmann, and J. Robertson, Appl. Phys. Lett. **95**, 173115 (2009).
[57] J. Dijon, P. D. Szkutnik, and A. Founrier, Carbon **48**, 3953 (2010).
[58] T. Hiraka, D. Futaba, and K. Hata, J. Am. Chem. Soc. **128**, 13338 (2006).
[59] T. De Los Arcos, Appl. Phys. Lett. **80**, 2382 (2002).
[60] C. Zhang, J. Appl. Phys. **108**, 024211 (2010).
[61] S. Esconjauregui, Appl. Phys. Lett. **95**, 173115 (2009).
[62] B. C. Bayer, J. Phys. Chem. C **115**, 4359 (2011).
[63] J. Robertson, G. Zhong, S. Hofmann, B. C. Bayer, H. Telg, and C. Thomsen, Diamond Relat. Mater. **18**, 957 (2009).
[64] M. Xu, D. N. Futaba, T. Yamada, M. Yumura, and K. Hata, Science **330**, 1364 (2010).

